

# Fast multigrid based computation of induced electric field for transcranial magnetic stimulation

Ilkka Laakso and Akimasa Hirata

Department of Computer Science and Engineering, Nagoya Institute of Technology, Japan

E-mail: laakso.ilkka@nitech.ac.jp

## Abstract.

In transcranial magnetic stimulation (TMS), the distribution of the induced electric field, and the affected brain areas, depend on the position of the stimulation coil and the individual geometry of the head and brain. The distribution of the induced electric field in realistic anatomies can be modelled using computational methods. However, existing computational methods for accurately determining the induced electric field in realistic anatomical models have suffered from long computation times, typically in the range of tens of minutes or longer. This paper presents a matrix-free implementation of the finite-element method with geometric multigrid method that can potentially reduce the computation time to several seconds or less even when using an ordinary computer. The performance of the method is studied by computing the induced electric field in two anatomically realistic models. An idealized two-loop coil is used as the stimulating coil. Multiple computational grid resolutions ranging from 2 to 0.25 mm are used. The results show that, for macroscopic modelling of the electric field in an anatomically realistic model, computational grid resolutions of 1 mm or 2 mm appear to provide good numerical accuracy compared to higher resolutions. The multigrid iteration typically converges in less than ten iterations independent of the grid resolution. Even without parallelization, each iteration takes about 1.0 s or 0.1 s for the 1 mm and 2 mm resolutions, respectively. This suggests that calculating the electric field with sufficient accuracy in real time is feasible.

PACS numbers: 87.10.Kn, 87.50.C-, 87.19.L-, 87.80.-y

Submitted to: *Phys. Med. Biol.*

## 1. Introduction

Transcranial magnetic stimulation (TMS) is a noninvasive technique for exciting the cortex or disturbing its function. In TMS, a strong pulse of electric current is passed through a coil that is placed over the scalp. The coil produces a time-varying magnetic field that penetrates into the head. The magnetic field induces an electric field that can depolarize cell membranes in the brain.

The distribution of the induced electric field, and the affected brain areas, depend not only on the positioning and orientation of the coil but also on the individual geometry of the head. The geometry of the head is heterogeneous, featuring various

tissue types with highly variable electrical properties. For instance, the electric field can be greatly affected by the distance between the scalp and cortex, distribution of the cerebrospinal fluid (CSF), and orientation of the gyri. Several recent studies have investigated the induced electric field in realistic models of the head and brain using computational techniques (Chen and Mogul 2010, Opitz *et al* 2011, Thielscher *et al* 2011, Sekino *et al* 2006, Salinas *et al* 2009, De Geeter *et al* 2011, Bijsterbosch *et al* 2012). However, high-resolution computer simulations may require restrictively long computation times in the range of tens of minutes to hours (De Geeter *et al* 2011, Windhoff *et al* 2012, Chen *et al* 2012). This limits the applicability of computational modelling towards personalized optimization of TMS coil positioning or real-time analysis of the induced electric field.

Computational methods for determining the induced electric field in heterogeneous anatomical models are based on the quasi-static approximation of Maxwell's equations. Under the quasistatic approximation, the TMS induced electric field can be represented in terms of the electric scalar potential which satisfies an elliptic partial-differential equation. The equation is discretized using finite-element or finite-difference methods and the resulting large linear equation system is solved numerically. One of the most efficient methods for solving such equation systems is the geometric multigrid method (Yavneh 2006), which has not yet been widely adopted in computational electromagnetics. The computational complexity of the geometric multigrid method is linear and it can be parallelized efficiently, making it superior to other methods for problems with a very large number of unknowns. The disadvantage of the geometric multigrid method is that, unlike for the case of generic matrix equation solvers, the implementation needs to be customized for each individual application, as the method exploits the structure of the underlying differential equation and geometry.

This paper presents a matrix-free implementation of the geometric multigrid method for the finite-element method (FEM) discretization of the electric scalar potential equation. Theory of multigrid methods has been studied extensively and is available elsewhere (see e.g. Yavneh (2006) for textbook references), so this paper will focus on how the method can be applied to electric field calculations in anatomically realistic models. The effectiveness of the method is demonstrated by computing the induced electric field in two anatomically based models. Particularly, we investigate the effects of computational voxel size and a sufficient convergence criterion that minimizes the computation time while providing good accuracy in computed electric field.

## 2. Computational methods

### 2.1. Finite element method for the scalar-potential equation

At low frequencies where the quasistatic approximation is valid, the electric scalar potential can be solved from (Wang and Eisenberg 1994)

$$\nabla \cdot \sigma \nabla \phi = -\nabla \cdot \sigma \mathbf{A}'_0, \quad (1)$$

where  $\phi$  is the induced electric scalar potential,  $\sigma$  is the conductivity and  $\mathbf{A}'_0$  is the time derivative of the magnetic vector potential. The induced electric field can be calculated from the gradient of the scalar potential by  $\mathbf{E} = -\nabla \phi - \mathbf{A}'_0$ .

Equation (1) can be discretized in various ways using finite-difference methods (Dawson *et al* 1996, Dawson and Stuchly 1998) or the FEM. The discretization in this

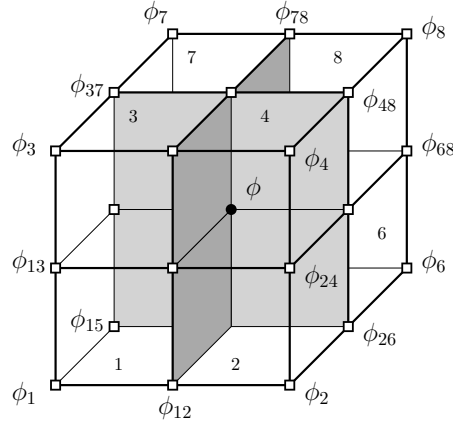


**Figure 1.** Eight voxels with the unknown nodal values at the corners. The voxels are labelled from 1 to 8. The subscripts of each nodal value denote the voxels that are adjacent to the node.

study employs the Galerkin FEM with trilinear node-based basis functions in cubical elements that correspond to the cubical voxels of the anatomical models, similarly to (Ilvonen and Laakso 2009). Because the elements form a regular grid, the elements of the FEM system matrix can be calculated analytically. Each row (corresponding to one node in the grid) of the resulting equation system is of the form

$$\frac{1}{h^2} \left( \frac{8}{3} \sigma_{12345678} \phi - \frac{1}{6} \underbrace{(\sigma_{12} \phi_{12} + \dots + \sigma_{78} \phi_{78})}_{12 \text{ terms}} - \frac{1}{12} \underbrace{(\sigma_1 \phi_1 + \dots + \sigma_8 \phi_8)}_{8 \text{ terms}} \right) \quad (2)$$

$$= \int \sigma \mathbf{A}'_0 \cdot \nabla \psi dV = f. \quad (3)$$

where  $h$  is the voxel side length,  $\phi$  is the unknown nodal value of the potential,  $\phi$  with subscripts are the potentials at the neighbouring nodes (figure 1),  $\sigma$  with subscript is the arithmetic average of the conductivity over the specified voxels in figure 1, and  $\psi$  is the piecewise trilinear basis function corresponding to the nodal value  $\phi$ . The integral  $f$  on the right-hand side can be calculated using numerical integration rules. In this work, the mid-ordinate integration rule (first-order Gaussian quadrature) is applied in the centre of each voxel. The boundary condition of zero normal component for the induced current on the surface of the body follows from (2) automatically, and does not need to be taken into account explicitly. The equation system consisting of equations of the form (2) is underdetermined up to a constant but still converges without problems because neither the residual of the solution nor the electric field depend on the constant term in the potential.

## 2.2. Geometric multigrid method

The geometric multigrid method is a method for solving linear equation systems that result from the discretization of elliptic partial difference equations, such as the scalar potential equation (1). The basic principle of the geometric multigrid method is to use multiple numerical grid sizes to speed up the convergence of the numerical solution. The following presents the outline of implementing the geometric multigrid method

---

**Algorithm 1** Geometric multigrid method for solving the FEM discretization of the scalar potential equation. The number of multigrid levels is  $L$ . SOR stands for the successive over-relaxation.

---

```

1: create 3D conductivity table  $\sigma^h$  from anatomical data
2: create the coarse grid conductivity tables  $\sigma^{2h}, \dots, \sigma^{2^{L-1}h}$ , from  $\sigma^h$ 
3: calculate source  $f^h$  from vector potential by (3)
4:  $\phi^h = 0$  (initial guess for the potential)
5: repeat
6:    $\phi^h = \text{V-cycle}(\phi^h, \sigma^h, f^h, h)$ 
7: until converged

8: procedure  $\phi^h = \text{V-cycle}(\phi^h, \sigma^h, f^h, h)$ 
9:    $\phi^h = \text{SOR}(\phi^h, \sigma^h, f^h, h, \nu = 3)$  ▷ Do  $\nu = 3$  steps of SOR.
10:   $r^h = \text{Residual}(\phi^h, \sigma^h, f^h, h)$  ▷ Calculate residual
11:   $f^{2h} = \text{Restrict}(r^h)$  ▷ Transfer the residual to coarse grid
12:   $\phi^{2h} = 0$  ▷ Initial guess for the coarse grid correction
13:  if  $\sigma^{2h}$  is the coarsest grid then
14:     $\phi^{2h} = \text{SOR}(\phi^{2h}, \sigma^{2h}, f^{2h}, 2h, \nu = 100)$  ▷ Coarsest grid level
15:  else
16:     $\phi^{2h} = \text{V-cycle}(\phi^{2h}, \sigma^{2h}, f^{2h}, 2h)$  ▷ Solve coarse-grid correction recursively
17:  end if
18:   $\phi^h = \phi^h + \text{Prolongate}(\phi^{2h})$  ▷ Transfer the correction to fine grid
19:   $\phi^h = \text{SOR}(\phi^h, \sigma^h, f^h, h, \nu = 1)$  ▷ Do  $\nu = 1$  steps of SOR.
20: end procedure

```

---

for solving the FEM discretization of the scalar potential equation in anatomically realistic voxel models. For more detailed theory and implementation, see e.g. Yavneh (2006), Hülsemann *et al* (2006), and the references therein.

In the following, the computational domain is assumed to be rectangular with dimensions  $l_x \times l_y \times l_z$ . The domain is divided evenly into cubical voxels with a side length of  $h$ . Table  $\sigma^h \in \mathbb{R}^{\frac{l_x}{h} \times \frac{l_y}{h} \times \frac{l_z}{h}}$  contains the conductivity values of each voxel. Likewise, tables  $\phi^h, r^h, f^h \in \mathbb{R}^{\frac{l_x+h}{h} \times \frac{l_y+h}{h} \times \frac{l_z+h}{h}}$  contain the nodal values of the potential, residual, and source term, respectively.

Algorithm 1 shows the flow of the geometric multigrid method for solving the scalar potential equation. The main part of the method is the V-cycle loop that consists of multiple progressive calls to successive over-relaxation (SOR), residual calculation, restriction, and prolongation operations. These operations and the generation of the coarse grids are briefly outlined in the following subsections. Note that, except for minor modifications described below, the principal structure of the V-cycle is practically unchanged from its textbook form (Yavneh 2006, Hülsemann *et al* 2006). In the usual implementation of the geometric multigrid method, the problem for the coarsest grid level on line 14 is solved exactly. In this work, this step was replaced by 100 steps of the SOR, which was observed to provide almost equally fast convergence with the benefit of slightly simpler implementation. Line 19 was skipped for the finest grid as it is directly followed by line 9 of the next iteration.

*2.2.1. Creating the coarse grids* In this work, it is assumed that anatomical data is represented in a regular grid of cubical voxels. Such a grid can be obtained by segmentation of anatomical images or from available ready-made anatomical models. Each voxel is assigned an electrical conductivity value that depends on the tissue type of the voxel. The resulting 3D table is the conductivity  $\sigma^h$  of the finest grid level for the geometric multigrid method. For implementation, it is useful to add empty layers around  $\sigma^h$  so that the grid size in each direction is divisible by  $2^{L-1}$ , where  $L$  is the number of multigrid levels.

The coarse-grid conductivity tables are constructed from the fine-grid conductivity such that each voxel in the coarse grid (voxel side length  $2h$ ) consists of eight fine-grid voxels ( $h$ ). The coarse conductivity  $\sigma^{2h}$  in each coarse-grid voxel is set to an arithmetic average

$$\sigma^{2h} = \frac{1}{8} \sum_{i=1}^8 \sigma_i^h,$$

where  $\sigma_i^h$  are the conductivity values of the eight fine-grid voxels that constitute one coarse grid voxel.

*2.2.2. SOR* One step of the elementary SOR iteration for the equation (2) is of the form: Visit all nodes in succession, and at each node do

$$\phi = (1 - \omega)\phi + \omega \frac{h^2 f + \frac{1}{6}(\sigma_{12}\phi_{12} + \dots + \sigma_{78}\phi_{78}) + \frac{1}{12}(\sigma_1\phi_1 + \dots + \sigma_8\phi_8)}{\frac{8}{3}\sigma_{12345678}}, \quad (4)$$

where the notation is similar to (2) and over-relaxation parameter  $\omega = 1.4$ . This value was found to provide good performance for a head-sized model.

*2.2.3. Residual* The residual is calculated by visiting all nodes in succession, and at each node residual  $r$  is set to

$$r = f - \frac{1}{h^2} \left( \frac{8}{3}\sigma_{12345678}\phi - \frac{1}{6}(\sigma_{12}\phi_{12} + \dots + \sigma_{78}\phi_{78}) - \frac{1}{12}(\sigma_1\phi_1 + \dots + \sigma_8\phi_8) \right), \quad (5)$$

where the notation is similar to (2).

*2.2.4. Restriction* Because of the node-based basis functions, the restriction operation that is used for transferring the residual from the fine grid to the coarse grid is full weighting, i.e., each nodal value in the coarse grid is an integral average of the fine-grid residual over eight voxels in the fine grid. Because the residual is piecewise trilinear, the residual everywhere over the eight voxels is determined by its values at the 27 nodes that correspond to the corners of the eight voxels. Hence, the integral average can be written as a weighted average of a total of 27 nodal values

$$f^{2h} = \sum_{i=1}^{27} C_i r_i^h,$$

where  $f^{2h}$  is the coarse grid source term. Terms  $r_i^h$  and  $C_i$  are the fine grid residual and the weighting factors at the 27 fine-grid nodes (figure 2).

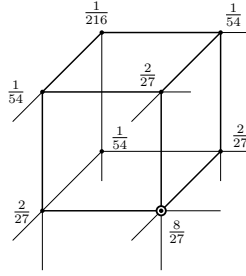


**Figure 2.** Weighting factors for the restriction operation in one octant of a cubical voxel (the centre of the voxel is lower right).

*2.2.5. Prolongation* The potential in the coarse grid is assumed to be node-based and piecewise trilinear, so the prolongation operation for transferring the potential from the coarse grid to the fine grid is (tri)linear interpolation

$$\phi^h = \text{Interpolate}(\phi^{2h}).$$

Consequently, the fine grid potential  $\phi^h$  at each node is an arithmetic average over either one, two, four, or eight nodal values of the coarse grid potential  $\phi^{2h}$ , depending on the node.

*2.2.6. Memory requirements* In the presented implementation, four large 3-D floating point tables are required: the conductivity (or multiple conductivity tables if tissue anisotropy is modelled), the unknown potential, the right-hand side source vector, and the residual. The same four tables are also required for all of the coarse grids which results in approximately 14% ( $1/8 + 1/64 + \dots$ ) increased memory requirements. In the case of anatomical head models, as much as 60% of the tables may be filled with air, which is not used in calculations, but takes up memory. Note that storing one vector field (such as the electric field or the vector potential) in the same grid would require three 3-D floating point tables. Therefore, if there is enough memory for processing the final electric field, then there should be no problems with memory during the simulation. With double-precision floating point numbers, a model of the head with 0.5 mm resolution requires at least 2.5 GB memory. Whenever the resolution is doubled (halved), the required memory is multiplied (divided) by eight.

### 2.3. Convergence analysis

In the following, the convergence of the numerical solution is reported in terms of the relative residual, which is defined as the Euclidean vector norm of the residual divided by the norm of the source term

$$\text{relative residual} = \frac{\|r^h\|_2}{\|f^h\|_2}.$$

The relative residual is a measure for the algebraic (or truncation) error of the solution of the equation system (2). The algebraic error is separate from the discretization error that results when the scalar potential equation (1) is replaced by its discrete counterpart using the FEM.

The final result, the induced electric field, is the gradient of the potential, so it is more sensitive to numerical error than the potential. The algebraic error of the electric field is investigated in terms of the maximum norm

$$\text{electric field error} = \frac{\max |\mathbf{E} - \mathbf{E}_{\text{ref}}|}{E_{99}},$$

where the maximum is taken over the whole head. The reference electric field  $\mathbf{E}_{\text{ref}}$  and the 99th percentile of its absolute value  $E_{99}$  (taken over the whole head) have been calculated from the potential converged to the machine precision. In practice, the error in the electric field can not be calculated during the iteration, as the reference electric field is not available. In this study, all simulations were performed two times: first, the reference electric field was determined and then, the convergence of the electric field was investigated.

#### 2.4. Measuring computation time

The computation time is reported in terms of the elapsed real time ('wall time'), not including any preprocessing steps (lines 1–4 in algorithm 1). In this work all simulations were run on the same workstation with a 12-core Intel Xeon X5690 processor running Ubuntu Linux. The presented simulation times are for the case when the code is run without parallelization using only single thread. The SOR, restriction and prolongation operations were implemented as MATLAB mex functions which were written in the C programming language and compiled using gcc version 4.6.3 with the `-Ofast` optimization flag. The main V-cycle loop, from which the mex functions were called, was implemented using MATLAB (version R2011b, MathWorks, Inc.). Double-precision floating point numbers were used.

### 3. Models

#### 3.1. TMS coil model

Several types of coil designs have been used for TMS (Deng *et al* 2012). Realistic TMS coils can be modelled using combinations of hundreds of infinitesimally short magnetic dipoles (Ravazzani *et al* 1996, Thielscher and Kammer 2002, Thielscher and Kammer 2004) or 3D models of coil wires (Salinas *et al* 2007, Bijsterbosch *et al* 2012).

Since the purpose of this work is not to investigate the effects of coil design, we have used an idealized figure-8 coil that consists of two circular current loops with a diameter of 5 cm. Each current loop has been modelled as a combination of 314 short magnetic dipoles, similarly to the study of Thielscher and Kammer (2004). More realistic coils could be modelled similarly (Thielscher and Kammer 2004, Thielscher *et al* 2011). Calculating the magnetic vector potential from the dipoles needs to be done only once for a single coil model, after which the vector potential for different coil positions can be obtained quickly by shifts and rotations. The figure-8 coil is positioned over the left hemisphere, roughly 3 cm left from the mid-sagittal plane at a height of 5 mm from the scalp. The position of the coil corresponds to no specific coil position in clinical or research applications. The coil current is assumed to vary sinusoidally at a frequency of 3 kHz.

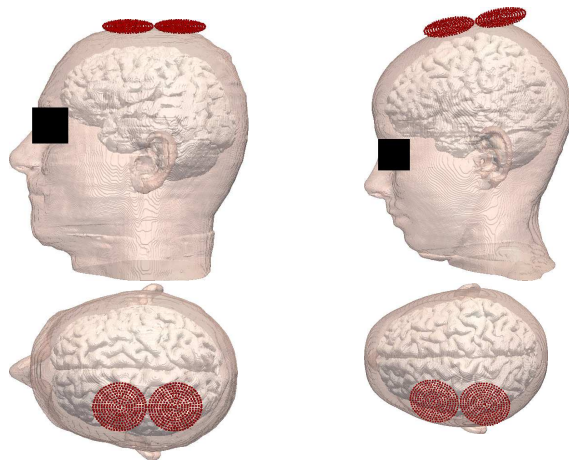


**Figure 3.** Position of the ideal figure-8 coil for the DUKE (left) and ELLA (right) models. The dots show the location of the dipoles that comprise the coil model.

### 3.2. Anatomical models

The TMS induced electric fields are determined in Caucasian male (DUKE) and female (ELLA) models (Christ *et al* 2010). Originally, the models comprise surface representation of tissues that has been constructed from MR images of a 34-year-old Caucasian male and 26-year-old Caucasian female. The same models have been used earlier for simulations of the TMS in the study of Bijsterbosch *et al* (2012). The original resolution of the MR images was  $0.5\text{ mm} \times 0.5\text{ mm} \times 1\text{ mm}$  (Christ *et al* 2010). For this work, three uniform rectangular grids of cubical voxels with side lengths 2 mm, 1 mm, and 0.5 mm have been extracted from the surface data. For investigating the effect of voxel size on the computation speed, an additional 0.25 mm resolution model has been created from the 0.5 mm model by dividing each voxel evenly into eight new voxels.

The models contain no information about possible anisotropy inside the voxels, so each voxel is assigned an isotropic conductivity value. The conductivities of tissue types at 3 kHz have been obtained from Gabriel’s four Cole-Cole model (Gabriel *et al* 1996). If the anisotropy of, for example, white matter were modelled, the overall structure of the method would stay unchanged, but minor modifications would be needed in discretization of the scalar-potential equation and coarse-grid generation.

A weakness of a rectilinear grid compared to a conformal tetrahedral mesh is that curved boundaries generally need to be modelled using staircase approximation. This results in spurious hotspots in the calculated electric field at tissue boundaries (Dawson *et al* 2002, Laakso and Hirata 2012b). In the study of Bijsterbosch *et al* (2012), the spurious electric field hotspots were removed by postprocessing. In this work, to prevent the generation of hotspots, the conductivity of the voxels was preprocessed similarly to our previous studies (Laakso and Hirata 2012b, Laakso and Hirata 2012a). The conductivity was smoothed by averaging it over a small sphere-like volume. For the resolutions of 2 mm, 1 mm, 0.5 mm, and 0.25 mm, the smoothing volumes were a star (seven voxels), a  $3 \times 3 \times 3$  cube (27 voxels), a  $5 \times 5 \times 5$  cube with rounded corners (93 voxels), and an approximately spherical volume (895 voxels), respectively. The smoothing was performed after line 1 in the multigrid algorithm (algorithm 1).

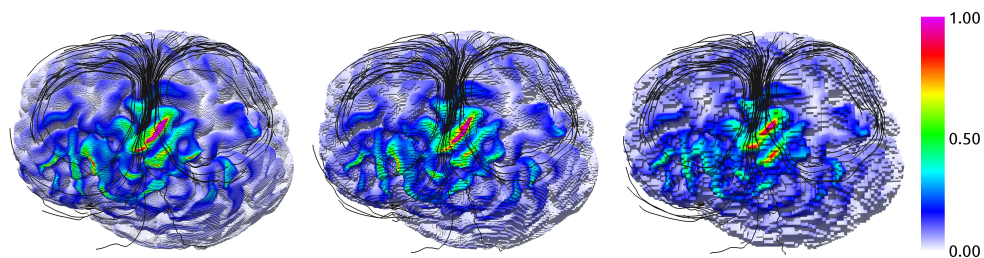


**Figure 4.** Normalized amplitude of the electric field on the surface of the cortex of the DUKE model for voxel sizes of 0.5 mm (left), 1 mm (middle), and 2 mm (right). Streamlines show the direction of the induced electric field in the head. The amplitude has been normalized such that the volume of brain tissue where the electric field is higher than 1.00 is  $0.04 \text{ cm}^3$  for the 0.5 mm voxel size.

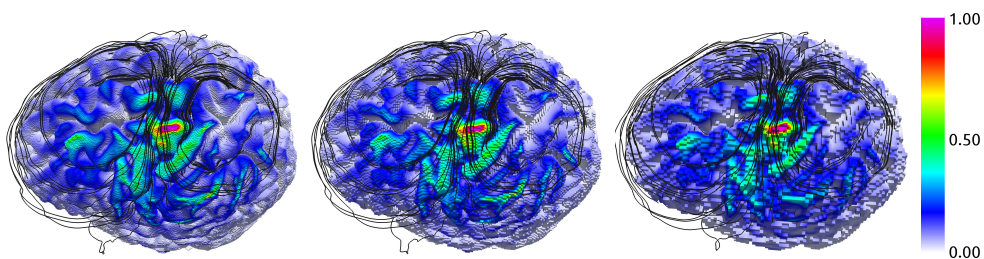


**Figure 5.** Normalized amplitude and direction of the induced electric field on the cortex of the ELLA model for voxel sizes of 0.5 mm (left), 1 mm (middle), and 2 mm (right).

#### 4. Results

The performance of the implemented code was verified by comparison with the analytic solution in a layered sphere exposed to the magnetic field of a short magnetic dipole. The results were exactly (to the machine precision) similar to those reported in our previous study (Laakso and Hirata 2012b).

Figures 4 and 5 show the electric field induced by the magnetic field of the figure-8 coil for voxel sizes of 0.5 mm, 1 mm, and 2 mm for the DUKE and ELLA models, respectively. At a glance, the distribution and direction of the induced electric field are similar for all voxel sizes. Compared to 0.5 mm and 1 mm voxel sizes, the 2 mm voxel size provides clearly coarser looking result, yet the locations of the peak electric fields and the direction of the induced current match closely those calculated with the finer voxel sizes. The highest cortical electric field occurs in the grey matter regions located under the centre of the stimulating figure-8 coil. The induced current primarily tends to flow in the CSF which has a much higher conductivity than grey or white matters. In locations where the orientation of the gyri is perpendicular to the direction of induced current, part of the current is forced to flow through the gyri. Due to the discontinuity of the normal component of the electric field on the CSF–cortex boundary, this results in several isolated regions with relatively high electric fields at some distance from the centre. This is in line with observations in earlier studies (Bijsterbosch *et al* 2012).

The focality of the electric field distribution for different voxel sizes is studied by selecting a small volume, e.g.  $1 \text{ cm}^3$ , and then determining a threshold value such

**Table 1.** Normalized electric field for both models with four voxel sizes. The electric field has been normalized such that, for a coil current of 1 A at a frequency of 3 kHz, the value of 1.00 corresponds to an electric field of  $7.1 \text{ mVm}^{-1}$  for the DUKE model and  $6.0 \text{ mVm}^{-1}$  for the ELLA model. The presented values are the threshold electric fields for volumes of 0.04, 0.2, 1.0, or  $5.0 \text{ cm}^3$ . This means that the electric field is higher than the threshold in a volume of 0.04, 0.2, 1.0, or  $5.0 \text{ cm}^3$  of brain tissue, and lower than the threshold elsewhere in the brain.

Model	Voxel size (mm)	Normalized threshold electric field			
		0.04 $\text{cm}^3$	0.2 $\text{cm}^3$	1.0 $\text{cm}^3$	5.0 $\text{cm}^3$
DUKE	2	0.91	0.73	0.48	0.32
	1	0.95	0.70	0.49	0.32
	0.5	1.00	0.72	0.49	0.32
	0.25	0.99	0.71	0.49	0.32
ELLA	2	1.02	0.73	0.48	0.33
	1	0.96	0.71	0.49	0.33
	0.5	1.00	0.72	0.49	0.33
	0.25	1.00	0.72	0.49	0.33

that the electric field is greater than or equal to the threshold in a volume of  $1 \text{ cm}^3$  of brain tissue, and lower than the threshold elsewhere in the brain. If the threshold decreases rapidly when the volume is increased, then the electric field distribution is concentrated in a small brain region. Table 1 shows the calculated threshold electric fields for volumes of 0.04, 0.2, 1.0, or  $5.0 \text{ cm}^3$  for both models and all four voxel sizes. As seen in the table, there are no significant differences in the electric field values between the voxel sizes. This, together with the results in figures 4 and 5, suggests that both the intensity and focality of the electric field distribution are relatively unaffected by the voxel size.

The convergence of the iteration in terms of the relative residual is shown in figure 6(left) and the truncation error of the electric field as a function of the relative residual is shown in figure 6(right). When allowing for a truncation error of 1% in the electric field, a sufficient stopping criterion for the iteration in terms of the relative residual seems to be in the order of  $10^{-5}$ . Probably due to geometrical artefacts, the electric field converges slower for the 1-mm DUKE model than for other voxel sizes or for the ELLA model. Other than that, the speed of convergence does not depend significantly on the voxel size, which is characteristic for multigrid methods. Although not presented here, we have studied multiple coil positions, and it seems that the speed of convergence does not depend significantly on the position of the stimulating coil.

Table 2 shows the number of unknowns and an efficient number of multigrid levels for both models and all four voxel sizes. The table also shows the number of multigrid V-cycles after which the truncation error in the electric field is less than 1% along with the computation time required for each V-cycle. For all voxel sizes, sufficient convergence is typically obtained in less than ten V-cycles. When using a single-threaded code, this means that a 2 mm head model can be solved in about 1 s, a 1 mm model in about 10 s, or a 0.5 mm model in about 1 min. Most of the computation time is spent for the SOR and calculation of the residual for the finest grid level. In practice, these operations could be made faster easily by parallelization or multithreading; the computation time was reduced to about one third when the SOR and calculation of the residual were multithreaded using OpenMP (2011).

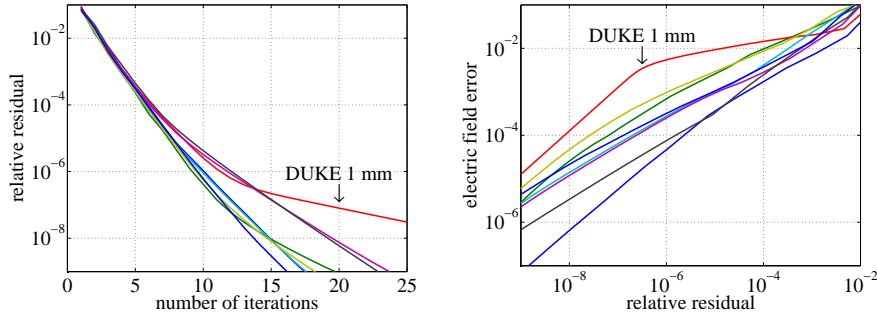


**Figure 6.** Convergence of the relative residual as the function of the number of iterations (left) and the error in the induced electric field as a function of the relative residual (right). Each curve represents a single case from a total of eight cases (two models with four voxel sizes). The only curve that differs significantly from the rest is the one for the DUKE model with the 1 mm voxel size.

**Table 2.** Number of unknowns, number of multigrid levels, and number V-cycle iterations after which the error in the electric field is less than 1%, along with the computation time required for one V-cycle.

Model	Voxel size (mm)	Unknowns (million)	Number of multigrid levels	Number of iterations	Time per iteration (s)
DUKE	2	0.66	4	4	0.13
	1	5.1	4	9	0.95
	0.5	40	5	5	6.89
	0.25	322	6	5	56.9
ELLA	2	0.56	4	6	0.11
	1	4.3	4	5	0.82
	0.5	34	5	6	5.93
	0.25	273	6	5	47.3

## 5. Discussion and conclusions

Implementation of the geometric multigrid method for solving the FEM discretization of the electromagnetic scalar potential equation was presented. The efficiency of the method was demonstrated by determining the TMS induced electric field in the head and brain in two anatomically realistic head models. Sufficient voxel size and convergence criterion were investigated.

The computation results showed that the coarse resolution of 2 mm provided a good approximation of the distribution and direction of the induced electric field. Regardless of the voxel size, sufficient convergence was typically obtained in less than ten V-cycle iterations. As the required time for one iteration was about 0.1 s or 1.0 s for the 2 mm and 1 mm voxel sizes, it is clear that computation of the electric field is fast enough for real time calculations on any modern computer, especially if the computational code were to be optimized further. Specifically, the multigrid method can be parallelized readily and efficiently (Hülsemann *et al* 2006, Schäfer 2006, Bergen *et al* 2006). Since the effectiveness of the multigrid method does not deteriorate when the number of unknowns increases, the method makes it possible to determine the

electric field with resolutions finer than currently available anatomical images. For example, calculating the electric field in a model of the whole head with a 250  $\mu\text{m}$  resolution took about 10 min, which could be further improved by parallelization.

Any potential applications of the method, such as planning or guiding the TMS coil placement and orientation, require numerical models of individual patient anatomies. There are automatic algorithms that can generate a patient-specific tetrahedral computational mesh from anatomical images in about 24 h (Windhoff *et al* 2012). Such kind of a mesh could be easily voxelized for use with the present code. However, as discussed by Windhoff *et al* (2012), it would be more straightforward to construct high-resolution rectilinear computational grid directly from imaging data, as done in e.g. Güllmar *et al* (2010). Note that the presented method is not limited to TMS: By altering the source term in (3), the method can be used for calculating the electric field during, for instance, transcranial direct or alternating current stimulation, deep brain stimulation, or stimulation of the spinal cord or peripheral nerves.

### Acknowledgements

The authors wish to thank the Finnish Cultural Foundation and the Academy of Finland for financial support.

### References

- Bergen B, Gradl T, Rude U and Hulsemann F 2006 A massively parallel multigrid method for finite elements *Computing in Science Engineering* **8**(6) 56–62
- Bijsterbosch J, Barker A, Lee K H and Woodruff P 2012 Where does transcranial magnetic stimulation (TMS) stimulate? Modelling of induced field maps for some common cortical and cerebellar targets *Med. Biol. Eng. Comput.* **50**(7) 671–81
- Chen M and Mogul D 2010 Using increased structural detail of the cortex to improve the accuracy of modeling the effects of transcranial magnetic stimulation on neocortical activation *IEEE Trans. Biomed. Eng.* **57**(5) 1216–26
- Chen X L, De Santis V, Chavannes N and Kuster N 2012 Computation of in situ electric field in the brain during transcranial magnetic stimulation *in* ‘Asia-Pacific International Electromagnetic Compatibility Symposium 2012’ pp. WE–AM–BIO1–3
- Christ A, Kainz W, Hahn E G, Honegger K, Zefferer M, Neufeld E, Rascher W, Janka R, Bautz W, Chen J, Kiefer B, Schmitt P, Hollenbach H P, Shen J, Oberle M, Szczerba D, Kam A, Guag J W and Kuster N 2010 The Virtual Family—development of surface-based anatomical models of two adults and two children for dosimetric simulations *Phys. Med. Biol.* **55**(2) N23–38
- Dawson T and Stuchly M 1998 High-resolution organ dosimetry for human exposure to low-frequency magnetic fields *IEEE Trans. Magnetics* **34**(3) 708–18
- Dawson T W, Caputa K and Stuchly M A 2002 Electric fields induced in humans and rodents by 60 Hz magnetic fields *Phys. Med. Biol.* **47**(14) 2561–8
- Dawson T W, Moerlose J D and Stuchly M A 1996 Comparison of magnetically induced ELF fields in humans computed by FDTD and scalar potential FD codes *Appl. Comput. Electromagn. Soc. J.* **11**(3) 63–71
- De Geeter N, Crevecoeur G and Dupre L 2011 An efficient 3-D eddy-current solver using an independent impedance method for transcranial magnetic stimulation *IEEE Trans. Biomed. Eng.* **58**(2) 310–20
- Deng Z D, Lisanby S H and Peterchev A V 2012 Electric field depth-focality tradeoff in transcranial magnetic stimulation: Simulation comparison of 50 coil designs *Brain Stimulation* **in press**(0)
- Gabriel S, Lau R W and Gabriel C 1996 The dielectric properties of biological tissues: III. Parametric models for the dielectric spectrum of tissues *Phys. Med. Biol.* **41**(11) 2271–93
- Güllmar D, Haueisen J and Reichenbach J R 2010 Influence of anisotropic electrical conductivity in white matter tissue on the EEG/MEG forward and inverse solution. a high-resolution whole head simulation study *NeuroImage* **51**(1) 145–63
- Hülsemann F, Kowarschik M, Mohr M and Rüde U 2006 *in* A. M Bruaset and A Tveito, eds,

- ‘Numerical Solution of Partial Differential Equations on Parallel Computers’Vol. 51 of *Lecture Notes in Computational Science and Engineering* Springer Berlin Heidelbergpp. 165–208
- Ilvonen S and Laakso I 2009 Computational estimation of magnetically induced electric fields in a rotating head *Phys. Med. Biol.* **54**(2) 341–51
- Laakso I and Hirata A 2012a Computational analysis of thresholds for magnetophosphenes *Phys. Med. Biol.* **57**(19) 6147–65
- Laakso I and Hirata A 2012b Reducing the staircasing error in computational dosimetry of low-frequency electromagnetic fields *Phys. Med. Biol.* **57**(4) N25–34
- OpenMP 2011‘Application program interface, version 3.1’  
**URL:** <http://www.openmp.org>
- Opitz A, Windhoff M, Heidemann R M, Turner R and Thielscher A 2011 How the brain tissue shapes the electric field induced by transcranial magnetic stimulation *NeuroImage* **58**(3) 849–59
- Ravazzani P, Ruohonen J, Grandori F and Tognola G 1996 Magnetic stimulation of the nervous system: Induced electric field in unbounded, semi-infinite, spherical, and cylindrical media *Annals of Biomedical Engineering* **24** 606–16
- Salinas F S, Lancaster J L and Fox P T 2007 Detailed 3D models of the induced electric field of transcranial magnetic stimulation coils *Phys. Med. Biol.* **52**(10) 2879–92
- Salinas F S, Lancaster J L and Fox P T 2009 3D modeling of the total electric field induced by transcranial magnetic stimulation using the boundary element method *Phys. Med. Biol.* **54**(12) 3631–47
- Schäfer M 2006in ‘Computational Engineering — Introduction to Numerical Methods’Springer Berlin Heidelbergpp. 277–306
- Sekino M, Hirata M, Sakihara K, Yorifuji S and Ueno S 2006 Intensity and localization of eddy currents in transcranial magnetic stimulation to the cerebellum *IEEE Trans. Magnetics* **42**(10) 3575–7
- Thielscher A and Kammer T 2002 Linking physics with physiology in TMS: A sphere field model to determine the cortical stimulation site in TMS *NeuroImage* **17**(3) 1117–30
- Thielscher A and Kammer T 2004 Electric field properties of two commercial figure-8 coils in TMS: calculation of focality and efficiency *Clinical Neurophysiology* **115**(7) 1697–708
- Thielscher A, Opitz A and Windhoff M 2011 Impact of the gyral geometry on the electric field induced by transcranial magnetic stimulation *NeuroImage* **54**(1) 234–43
- Wang W and Eisenberg S 1994 A three-dimensional finite element method for computing magnetically induced currents in tissues *IEEE Trans. Magnetics* **30**(6) 5015–23
- Windhoff M, Opitz A and Thielscher A 2012 Electric field calculations in brain stimulation based on finite elements: An optimized processing pipeline for the generation and usage of accurate individual head models *Hum. Brain Mapp.* **in press**
- Yavneh I 2006 Why multigrid methods are so efficient *Computing in Science Engineering* **8**(6) 12–22